PHYSICS

Deep learning of quantum entanglement from incomplete measurements

Dominik Koutný[1]*, Laia Ginés[2], Magdalena Moczała-Dusanowska[3], Sven Höfling[4], Christian Schneider[5], Ana Predojević[2], Miroslav Ježek[1]*

The quantification of the entanglement present in a physical system is of paramount importance for fundamental research and many cutting-edge applications. Now, achieving this goal requires either a priori knowledge on the system or very demanding experimental procedures such as full state tomography or collective measurements. Here, we demonstrate that, by using neural networks, we can quantify the degree of entanglement without the need to know the full description of the quantum state. Our method allows for direct quantification of the quantum correlations using an incomplete set of local measurements. Despite using undersampled measurements, we achieve a quantification error of up to an order of magnitude lower than the state-of-the-art quantum tomography. Furthermore, we achieve this result using networks trained using exclusively simulated data. Last, we derive a method based on a convolutional network input that can accept data from various measurement scenarios and perform, to some extent, independently of the measurement device.

INTRODUCTION

Physical measurements performed on individual parties of an entangled system reveal strong correlations (1), which give rise to nonclassical and nonlocal effects (2, 3). Aforesaid effects are the essential element of fundamental tests of quantum mechanics, including direct experimental verification of quantum nonlocality (4–6). The critical role of entanglement was demonstrated also on the opposite scale of the complexity spectra in macroscopic phase transitions (7–9). Besides the fundamental aspects, entanglement is an essential tool for quantum information processing, and it allows for reaching the quantum advantage (10, 11). Modern quantum communication networks rely crucially on entanglement sources (12–15). Consequently, the characterization of entanglement is paramount for both fundamental research and quantum applications (16, 17).

Here, we adopt methods of deep learning to tackle the long-standing problem of efficient and accurate entanglement quantification. Our approach determines the degree of entanglement of a generic quantum state directly from an arbitrary set of local measurements. Despite the deep learning models being trained on simulated measurements, they excel when applied to real-world measurement data. We quantify photonic entanglement generated by two distinct systems: a nonlinear parametric process and a semiconductor quantum dot.

Reliable entanglement quantification represents an open problem in quantum physics. Direct measurement of entanglement can be achieved by exploiting quantum interference of two (or more) identical copies of a physical system (18–22). This multicopy approach roots in measuring nonlinear functions of quantum states

(23, 24). However, such measurements are experimentally highly demanding, which has spurred the research of single-copy entanglement detection using only local measurements, such as quantum tomography.

Quantum tomography provides the full description of a quantum state including the degree of entanglement (25, 26). However, the total number of measurements required for quantum tomography increases exponentially with the number of qubits or quantum degrees of freedom, which renders the approach inherently not scalable (27–29). Several methods have been developed to make this scaling more favorable, nevertheless, by imposing an a priori structure or symmetry to the system (30–33). When a few-parameter model of quantum state is assumed, quantum estimation can be used for optimal inferring of the state entanglement (34–36). Another approach to emulate quantum correlations (37) with fewer resources relies on neural network quantum states (38–42). However, this method suffers from the sign problem, solving of which requires further assumptions about the state (43, 44). The neural network quantum state approach was used for quantum tomography under nonideal experimental conditions (45–49). However, how much information is needed for representing a generic quantum state at a given level of accuracy remains an open question (50, 51).

Instead of characterizing the whole system, one might target only mean values of a set of selected observables, which substantially reduces the required number of measurements. This approach, termed shadow tomography (52), can also be applied to estimate entanglement entropy of a small subsystem, basically reconstructing its reduced quantum state (53, 54). An alternative method uses random measurements to estimate the second-order Rényi entropy of a subsystem (55–58). However, quantification of entanglement distributed over the whole system lies beyond the scope of such methods.

Entanglement witnessing seems to be a viable alternative to the tomographic methods, when we only aim at distinguishing between entangled and nonentangled states (or between entanglement classes) without quantifying the degree of entanglement and its

[1]Department of Optics, Faculty of Science, Palacký University, 17. listopadu 12, 77146 Olomouc, Czechia. [2]Department of Physics, Stockholm University, 10691 Stockholm, Sweden. [3]Princeton Institute of Materials, Princeton University, Princeton, NJ 08544, USA. [4]Technische Physik, Physikalisches Institut and Würzburg-Dresden Cluster of Excellence ct.qmat, Universität Würzburg, Am Hubland, D-97074 Würzburg, Germany. [5]Institute of Physics, University of Oldenburg, D-26129 Oldenburg, Germany.
*Corresponding author. Email: koutny@optics.upol.cz (D.K.); jezek@optics.upol.cz (M.J.)

detailed structure. Nevertheless, the witnessing may still require the full knowledge of the underlying quantum state, as is the case of the positive partial transpose criterion (*1*). The witness cannot be directly measured; however, it can be approximated using a completely positive map (*59*), which is equivalent to the full quantum state tomography (*60, 61*). Other witnessing methods are based on the minimum local decomposition (*62, 63*), semidefinite programming (SDP) (*64, 65*), entanglement polytopes (*66*), or correlations in random measurements (*67, 68*). Entanglement witnessing can also be facilitated by using neural networks classifiers (*69–71*). Despite the success of the entanglement witnessing, it provides only witnesses or lower bounds and often requires some a priori information about the state.

In summary, the connection between the entanglement present in a physical system and the measurements of the correlations of its subsystems is highly nontrivial (*72, 73*). It seems that full entanglement characterization using single-copy local measurements can only be accomplished with the complete quantum state tomography

and, consequently, with exponential scaling of the number of required measurements (*60, 61, 74, 75*). The open question remains what one can learn about entanglement from an incomplete observation.

In this work, we use deep neural networks (DNNs) to tackle the problem of entanglement characterization. We develop a method that allows us to quantify the degree of entanglement and quantum correlations in a generic partially mixed state using a set of informationally incomplete measurements. The entanglement quantifiers that we obtain using DNN approach are substantially more accurate compared with the values attainable using the state-of-the-art quantum tomography methods. In addition, we demonstrate a measurement-independent quantification of entanglement by developing a deep convolutional network that accepts an arbitrary set of projective measurements without retraining. The DNN-based approaches that we introduce here can be immediately applied for certification and benchmarking of entanglement sources, which we demonstrate by using photonic sources of entangled photons based on spontaneous parametric downconversion and a semiconductor quantum dot.

RESULTS

Even in a well-understood system, such as a pair of qubits, a reliable quantification of entanglement requires full state tomography (*74*). In other words, to infer the degree of entanglement, we need to determine the quantum state. A common approach to implement photonic qubit tomography is to measure the full basis of three Pauli operators. Such a measurement for a two-qubit state consist of $6^2 = 36$ local projectors (*26*). Omitting randomly some projectors in this measurement scheme decreases the accuracy of the quantum tomography and, consequently, the entanglement evaluation. Here, we show that this problem can be overcome by using DNNs that allow us to gain knowledge on the degree of entanglement without the need to know the quantum state.

To demonstrate the advantage of the DNN approach, we use two quantifiers: the concurrence (*1*) and the mutual information (*76*) for a two-qubit and a three-qubit system, respectively. The concurrence is widely used in experiments for characterization of entangled photon pair sources. Its value is bounded from below by 0 for separable states and from above by 1 for maximally entangled states. On the other hand, the concurrence cannot be easily generalized to higher-dimensional quantum systems and systems of more than two parties. Therefore, the second quantifier that we use is the mutual information, which can be generalized to multipartite systems of qudits, and its value reflects the information shared between the parties of a larger system.

We use three different approaches to determine the concurrence and the mutual information from an incomplete set of data. We show them schematically in Fig. 1. We use the maximum likelihood algorithm (MaxLik) (Fig. 1A, red), measurement-specific DNNs (Fig. 1B, green), and a measurement-independent DNN (Fig. 1C, blue). The maximum likelihood is an algorithm that finds the quantum state (ρ) iteratively, starting from an initial guess (ρ_{init}), which is typically set to maximally mixed state (*77*). Having at hand the quantum state ρ allows us to quantify the entanglement (see Materials and Methods). In contrast, the approaches based on DNN learn the concurrence and mutual information directly from the measured data. While the measurement-specific DNN is
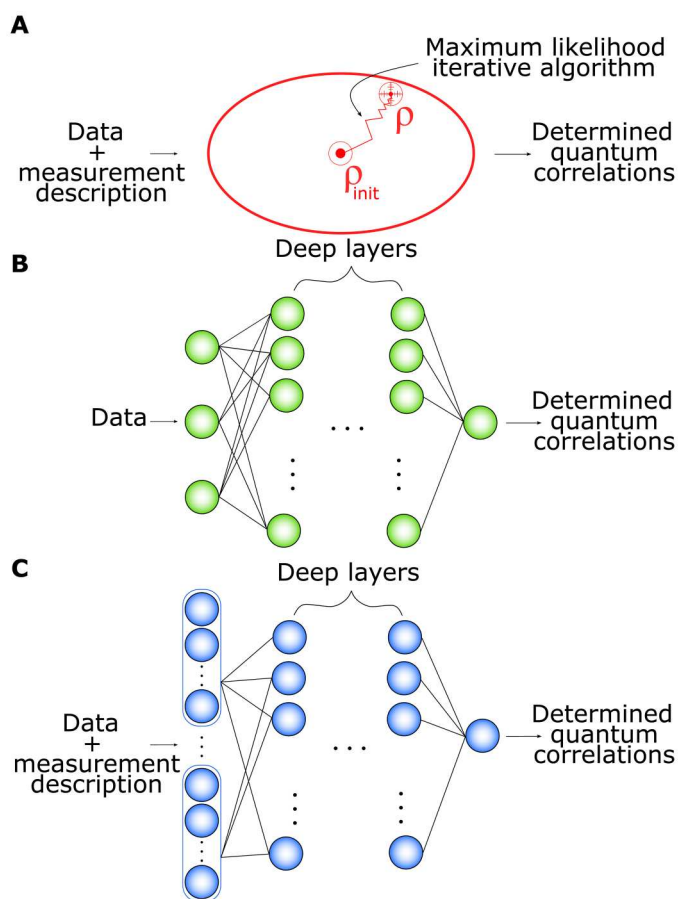

Fig. 1. Schematics of the three methods that we used to infer the quantum correlations. (**A**) The maximum likelihood algorithm (MaxLik) finds the most likely quantum state ρ based on the measured data and an initial guess ρ_{init}. (**B**) Green DNN represents a fully connected neural network that infers directly the concurrence and the mutual information from specific measurements (specific measurement projectors), whereas (**C**) the blue DNN works with an arbitrary measurement projectors. The input for the former is the measured data. The measurement-independent DNN has a first layer convolutional, and it inputs both the data and the measurement description.

designed for a predefined set of measurement projectors M_m, the measurement-independent DNN relaxes the condition on measuring the a priori known projectors and predicts concurrence and mutual information independently on the measurement settings. This approach has a convolutional first layer, and it inputs the measured data together with the description of the respective projectors. During the training, the DNNs are provided with the theoretical probabilities $\mathrm{Tr}\{\rho M_m\}$ and, in the case of the measurement-independent DNN, also the description of the measurement M_m. For the detailed information about the structure of the DNNs, the dataset, and the training procedure, see Materials and Methods.

We compare the three approaches on the basis of how accurately they can infer the concurrence (mutual information) from an incomplete set of data. Here, the MaxLik serves as a benchmark to the other two methods that are DNN-based. We chose to evaluate the performance of all three approaches by computing the mean absolute error (MAE). The MAE is calculated as $\langle|x_i - y_i|\rangle$ with x_i being the true value and y_i being the predicted value of the concurrence (mutual information). To make our comparison universal, the average is taken over a set of states and several combinations of measurement projectors, i.e., a test set. The total number of combinations of k projectors from the maximum of 36 is $\frac{36!}{k!(36-k)!}$. As this number can be excessively high, we randomly selected a smaller subset of combinations. Therefore, to evaluate the performance of a measurement-specific DNN, we train 12 randomly selected networks for each k-projector measurement and evaluate the average and SD of their MAEs. For the MaxLik and measurement-independent DNN, the averaging is performed over hundreds of randomly selected measurements.

The performance of the three approaches is presented in Fig. 2, where we show how MAE depends on the number of measurement projectors that we used to obtain the result. Figure 2 (A and B) shows the MAE for the concurrence and the mutual information, respectively, while Fig. 2C addresses the MAE of the three-qubit mutual information matrix. The MaxLik approach is presented using the red triangles in all panels. For the informationally complete data, i.e., when all 36 projectors are measured, the MaxLik MAE is on the order of 10^{-5} to 10^{-4}. In this scenario, MaxLik converges to the true quantum state, and the error only reflects the numerical errors caused by the computing precision. As we can see in Fig. 2 (A and B), the MAE of the MaxLik starts increasing if only a

few out of the 36 projectors are absent. In contrast to the MaxLik, DNNs perform well even for a severely reduced number of projectors. The measurement-specific DNNs (shown in green circles) predict the concurrence and mutual information with the MAE of approximately 0.01 even when only 24 projectors are used. For the same number of projectors, MaxLik MAE is 0.1. Consequently, measurement-specific DNNs result in a precision that is, on average, 10 times higher. If we further reduce the number of projectors, then the MAE for the measurement-specific DNNs starts to increase; however, it keeps being substantially smaller compared to the MAE of the MaxLik. The uncertainty region of MAE also remains at least two times smaller (up to 10 times while working with more than 18 projectors). The measurement-independent DNN error is shown in Fig. 2 using the blue squares. Compared to the performance of the MaxLik, the measurement-independent DNN quantifies the concurrence and the mutual information with a lower MAE however worse than using the measurement-specific strategy. In practice, one can resource to the measurement-independent DNN for preliminary detecting the entanglement in the system, even changing the measurement on the fly, and improve the entanglement quantification by training a particular measurement-specific DNN later.

To further validate our approach, we compare the values of the concurrence determined by MaxLik, measurement-specific DNNs, and measurement-independent DNN using a state that the network has never seen before, the Werner state $\rho_W(p) = p\rho_{\psi^-} + \frac{1-p}{4}\mathbb{1}$, where ρ_{ψ^-} is a projector into maximally entangled Bell state spanning the asymmetric subspace of two qubits. The parameter p runs from 0 (mixed state) to 1 (maximally entangled state). The concurrence for the Werner state is a piecewise linear function of the parameter p, and it takes the exact form $C(\rho_W) = \max[0, (3p-1)/2]$. The results are shown in Fig. 3. In the panels (A to D), we show the concurrence and the corresponding uncertainty regions for 36, 28, 18, and 8 projective measurements, respectively. For 28 and 18 measurement projectors, both the DNN approaches follow the ideal concurrence values, while the MaxLik deviates substantially. The measurement-specific DNNs yield nontrivial results even in the case of only 8 measurement projections.

As mentioned previously, the mutual information can be generalized to the systems of more than two qubits. To show that we can also generalize the DNN-based approach to larger quantum
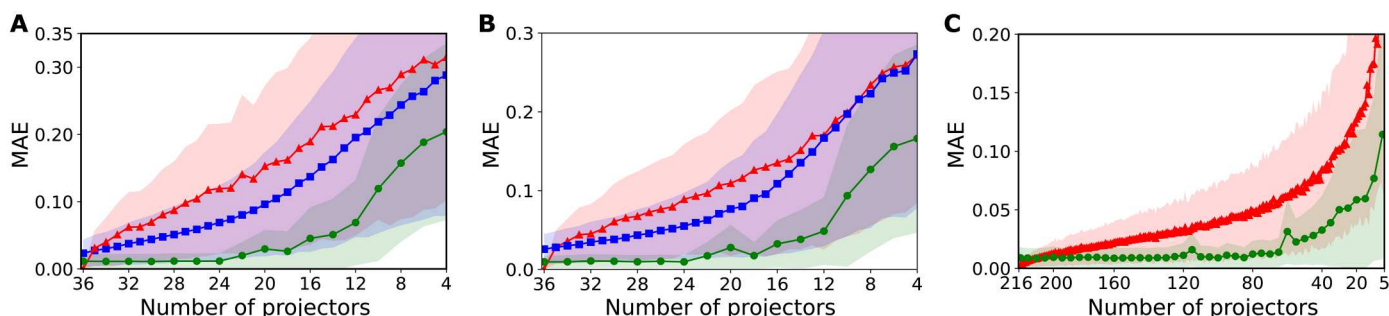

Fig. 2. Entanglement quantification error for the two- and three-qubit systems. The mean absolute error (MAE) versus the number of measurement projectors for (**A**) two-qubit concurrence, (**B**) two-qubit mutual information, and (**C**) three-qubit mutual information matrix. Red triangles depict MAE for the MaxLik, blue squares stand for the values of MAE computed from measurement-independent DNN, and, lastly, green circles represent the values of MAE computed from measurement-specific DNNs. The uncertainty regions are depicted in the corresponding colors and may overlap. The DNNs outperform the MaxLik approach in terms of entanglement quantification accuracy and its consistency, given by smaller errors and uncertainty intervals, even for substantially incomplete measurements.
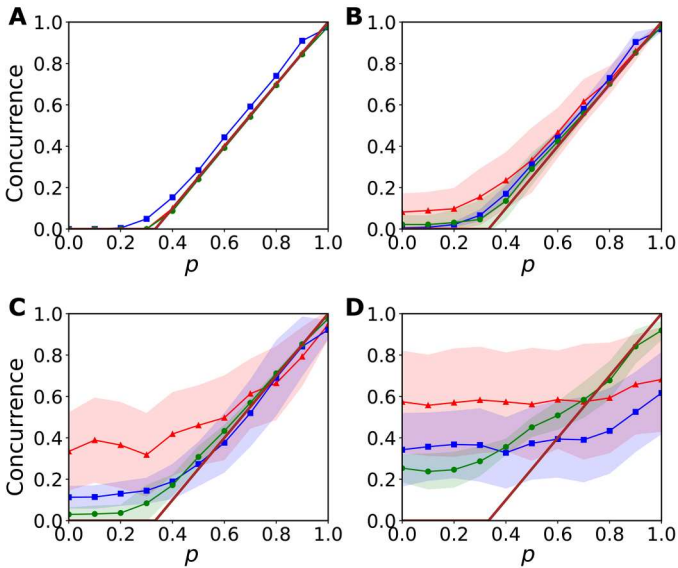
Fig. 3. Entanglement quantification error for the Werner state. The dependence of values of concurrence for the two-qubit Werner state $\rho_W(p)$ characterized by the parameter $p \in [0,1]$. Values of the concurrence determined from (**A**) 36, (**B**) 28, (**C**) 18, and (**D**) 8 measurement settings. In each panel, the red triangles depict the average values of the concurrence determined by the MaxLik with corresponding uncertainty region, the blue squares stand for the measurement-independent DNN predictions, and the green circles represent predictions given by measurement-specific DNNs. The brown line shows the theoretical values of the concurrence for the Werner state. Both measurement-independent DNN and measurement-specific DNNs outperform the MaxLik in entanglement quantification of the Werner state.

systems, we apply our method to a three-qubit system. In such a system, the mutual information matrix has three independent entries $\mathscr{I} \equiv \{\mathscr{I}_{AB}, \mathscr{I}_{AC}, \mathscr{I}_{BC}\}$, with subscripts referring to the three different ways of partition. To determine all three numbers $\mathscr{I}$ simultaneously, we have to perform a full tomographic measurement on each qubit, which leave us with $6^3 = 216$ projections. Following the procedure introduced for the two-qubit case, we built measurement-specific DNNs, each mapping measurement data to

Table 1. The summary of the mutual information quantification from incomplete measurements consisting of one-fourth of all possible Pauli projectors in each case. The MaxLik and the measurement-specific DNNs are compared up to five-qubit quantum systems. The ratio of the mean absolute errors (MAEs) of the methods shows an increasing improvement in the performance of the DNN approach for entanglement quantification in higher-dimensional systems.

Number of qubits	MAE		Ratio of MaxLik and DNN MAEs
	MaxLik	**DNN**	
2	0.20 ± 0.16	0.09 ± 0.09	2.2
3	0.068 ± 0.055	0.023 ± 0.020	3.0
4	0.019 ± 0.014	0.005 ± 0.001	3.8
5	0.039 ± 0.032	0.009 ± 0.001	4.3

the three-component vector $\mathscr{I}$. Deep layers have the same structure as for quantification of mutual information in the two-qubit case. Final results are shown in Fig. 2C. The MAE of $\mathscr{I}$ is averaged over its three independent elements and over randomly generated quantum states. DNN predictions are, on average, akin to the MaxLik ones in the regime close to the complete data. However, with only about a third of all projections, measurement-specific DNNs predict the full mutual information matrix on average with a five times smaller error than the MaxLik.

Our approach needs modest computational resources. In particular, the two- and three-qubit measurement-specific networks (for one-fourth of all Pauli projectors compared to the complete measurement) have approximately 37,000 and 42,000 parameters, respectively. The optimal performance of networks for three qubits does not require substantially more parameters than for two-qubit networks. We further verified this optimistic scaling by training four- and five-qubit measurement-specific networks (for one-fourth of all possible Pauli projectors in each case). These networks require 69,000 and 231,000 parameters, respectively, and outperform the MaxLik even more than two-qubit and three-qubit networks; see Table 1. Namely, the measurement specific networks reach 2.2, 3.0, 3.8, and 4.3 times lower MAE of mutual information matrix than the MaxLik for two, three, four, and five qubits, respectively. On the basis of this finding, we expect that, by keeping the ratio of the MaxLik accuracy and the DNN accuracy constant, the required fraction of the projectors with respect to the full tomography will decrease.

Last, we demonstrate the performance of DNN-based entanglement quantification using experimental data acquired under nonideal conditions and with limited statistical sampling. We study two distinct entanglement sources. The first one is based on continuously pumped spontaneous parametric downconversion. The photon pair generation process is inherently random, and the resulting entangled state depends on the choice of the temporal coincidence window and other experimental conditions such as background noise. Adjusting of the experimental parameters affects the degree of entanglement in the produced state. We quantify concurrence using the DNNs and the MaxLik approach for various experimental settings ranging from the maximally entangled singlet Bell state to a noisy state with a negligible concurrence. Figure 4 (A and B) shows the results for an almost pure entangled state and a partially mixed state with the concurrence of 0.985 ± 0.001 and 0.201 ± 0.002, respectively. In both cases, DNN approaches outperform the MaxLik approach. The measurement-specific DNNs remain very accurate (MAE <0.04) all the way down to 14 projections. Even the measurement-independent DNN outperforms the MaxLik in the generic case of partially mixed state for any number of measurement projectors. The maximally entangled state represents the only case where the MaxLik performs slightly better than the measurement-independent DNN (but worse than measurement-specific DNNs). This behavior results from high purity and sparsity of the state and, consequently, from the sparsity of the measurement data. When randomly selecting a subset of projectors, there is a high possibility of having a majority or even all the measurements with a negligible number of detection counts. It seems that the predictive strength of the measurement-independent DNN is limited for such a scenario. However, the MaxLik approach is biased toward pure states in the case of heavily undersampled data (*78, 79*), and the positivity constraint tends to a sparse (low-rank)
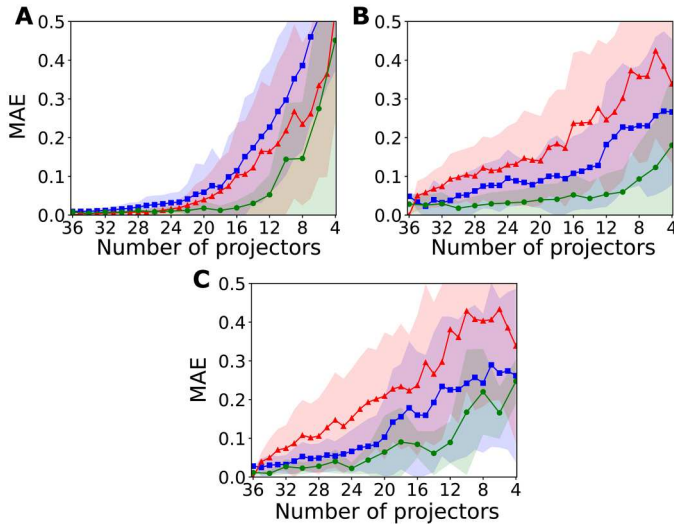
Fig. 4. Performance of MaxLik and DNN-based approaches for an experimental datasets. We show the dependence of the MAE on the number of projectors. (**A** and **B**) Spontaneous parametric downconversion sources and (**C**) semiconductor quantum dot source. The concurrence of experimentally prepared quantum states was determined from the full MaxLik tomography to (A) 0.985 ± 0.001, (B) 0.201 ± 0.002, and (C) 0.18 ± 0.01. The MAE for the measurement-specific DNNs is depicted in green circles, for measurement-independent DNN in blue squares, and for the MaxLik approach in red triangles.

states (*80*). This bias artificially increases the resulting concurrence and reduces its error.

The second experimental system consists of a semiconductor quantum dot resonantly pumped by picosecond pulses. The biexciton-exciton cascade emission produces pairs of photons in a partially polarization entangled state. The degree of entanglement is reduced by the presence of the fine-structure splitting, reaching the concurrence of 0.18 ± 0.01. Figure 4C shows the MAE for such a mixed quantum state. As for the source based on spontaneous downconversion, both DNN approaches beat, on average, the MaxLik method in accuracy. Let us point out that the DNN-based approaches were trained to predict quantum correlations from the theoretical probabilities computed from the ideal quantum states and measurement. Figure 3 thus demonstrates the robustness of our approaches to noisy experimental data.

DISCUSSION
We demonstrated that, by exploiting novel methods of neural networks and deep learning, we can outperform the traditional and commonly used techniques for quantification of quantum correlations such as state tomography. For the systems of two qubits, we built two different neural network–based approaches, namely, measurement-specific and measurement-independent DNNs. Both approaches predict concurrence and mutual information from data with a higher accuracy than the commonly used quantum state tomography. The best performing approach is the measurement-specific DNNs, which are trained to predict the concurrence or mutual information from a fixed set of projectors. Furthermore, we generalized to the system of three qubits, where we show that the measurement-specific DNNs represent a more accurate method to

quantify the mutual information matrix than the maximum likelihood one. We demonstrated the feasibility of the measurement-specific DNNs training up to five qubits. Our approaches not only benefit from a high accuracy when working with fewer measurement projectors but also are substantially faster compared to the standard tomography–based methods. Furthermore, we demonstrate the robustness of our approach using two experimental systems: a nonlinear parametric process and a semiconductor quantum dot. The DNN approaches can be further studied and modified to adaptively find a minimal set of projectors that infer the entanglement accurately.

MATERIALS AND METHODS
Quantifying quantum correlations
To quantify the quantum correlation, we use the concurrence and the mutual information, for the two- and three-qubit cases, respectively. The concurrence is a two-qubit monotone entanglement measure (*1*) widely used for the characterization of bipartite entanglement commonly present in sources of entangled photon pairs. Knowing the quantum state the concurrence is defined as

$$\mathscr{C}(\rho) \equiv \max\{0, \lambda_1 - \lambda_2 - \lambda_3 - \lambda_4\} \tag{1}$$

with $\lambda_1, ..., \lambda_4$ being the eigenvalues (sorted in decreasing order) of the Hermitian matrix $T = \sqrt{\sqrt{\rho}\tilde{\rho}\sqrt{\rho}}$, here $\tilde{\rho} = \sigma_y \otimes \sigma_y \rho^* \sigma_y \otimes \sigma_y$, where ρ^{*} standing for complex conjugate and σ_y is one of the Pauli matrices represented in a computational basis as $\sigma_y = i(|1\rangle\langle 0| - |0\rangle\langle 1|)$. For an arbitrary mixed state, the value of concurrence is saturated from below by 0 (*1*) for the separable states $\rho_{AB} = \sum_i \gamma_i \rho_A^i \otimes \rho_B^i$ and from above by 1 for the maximally entangled states of two-qubits.

Mutual information is a quantum correlation measure commonly used in quantum cryptography or for quantifying complexity in many-body systems. For an *n*-qubit quantum system, mutual information matrix reads

$$\mathscr{I}_{ij} = \frac{1}{2}[\mathscr{S}(\rho_i) + \mathscr{S}(\rho_j) - \mathscr{S}(\rho_{ij})] \tag{2}$$

and is constructed from the one and two point von Neumann entropies (*76*), $\mathscr{S}(\rho_i) = -\text{Tr}\{\rho_i \log_d \rho_i\}$ and $\mathscr{S}(\rho_{ij}) = -\text{Tr}\{\rho_{ij} \log_d \rho_{ij}\}$, with ρ_i and ρ_{ij} standing for reduced density matrices, $\rho_i = \text{Tr}_{k \neq i}\{\rho\}$ and $\rho_{ij} = \text{Tr}_{k \neq ij}\{\rho\}$ respectively.

Quantum state tomography
Quantum state tomography is a method to solve the inverse problem of reconstruction of an unknown quantum state. It uses the set of measurement operators (projectors) and relative frequencies $\{f_i\}$ acquired in a measurement. To obtain an informationally complete measurement, we need the relative frequencies for at least $D^2 - 1$ independent projectors $\{M_i\}_{i=0}^{N}$. Quantum state is reconstructed by maximizing the log-likelihood functional $\mathscr{L}(\rho) \propto \sum_{j=1}^{N} f_j \log p_j(\rho)$, which can be written (*77, 81, 82*) as the iterative map $\rho^{(k+1)} \leftarrow \mu_k R \rho^{(k)} R$, where μ is the normalization constant and R is an operator defined as $R = \sum_i f_i/p_i M_i$. Here, f_i are the measured frequencies and p_i are the theoretical probabilities given by the Born's rule $p_i = \text{Tr}\{\rho M_i\}$. In the Results section of this paper, we address how the measurement being incomplete affects the quantification accuracy of the concurrence and the mutual

information. In such a case, the closure relation, $\sum_i M_i = 1$, is no longer fulfilled. The optimal strategy is to map the set of projectors $\{M_i\}$ into a new set $\{M_{i'}\}$ via $M_{i'} = G^{-1/2}M_iG^{-1/2}$ with $G = \sum_i M_i$. One can easily check that the $\{M_{i'}\}$ now fulfill the completeness relation, $\sum_i M_{i'} = 1$. The iterative map then updates to

$$\rho^{(k+1)} \leftarrow \mu_k G^{-1/2}R\rho^{(k)}RG^{-1/2} \qquad (3)$$

and represents a procedure that we follow in the main text. We consider measurement settings to be the Pauli projectors, i.e., projectors into eigenstates of Pauli operators $\{\sigma_x, \sigma_y, \sigma_z\}$. The MaxLik estimator ρ^{MaxLik} is defined as a fixed point of the iterative map (Eq. 3). The iteration process starts from the completely mixed state $\rho_{\mathrm{init}} = 1/D$ and is stopped when the Hilbert-Schmidt distance between the subsequent iterations reaches 10^{-16}. In the case of encoding qubit states into the polarization degrees of freedom, Pauli measurement consists of projectors onto three mutually unbiased basis sets $\{|H\rangle\langle H|, |V\rangle\langle V|, |D\rangle\langle D|, |A\rangle\langle A|, |R\rangle\langle R|, |L\rangle\langle L|\}$.

There are other methods for quantum state tomography such as maximum likelihood–maximum entropy (83), SDP (84), or compressed sensing (30). These methods and their comparison to MaxLik and DNNs are presented in the Supplementary Materials.

DNN methods

Neural networks are machine learning models that learn to perform tasks by analyzing data. A DNN model consists of multiple layers of interconnected artificial neurons and acts as a highly nonlinear transformation parameterized by a large number of trainable parameters (85). DNNs have the ability to generalize from learning stage, i.e., once trained they can perform unexpectedly well even for inputs that were not observed during the learning stage. The basic principles of DNNs operation are well known, but the full span of their generalization ability is the subject of current research (86, 87). In science and technology, neural networks have been successfully applied to a wide range of problems, including predicting the behavior of complex systems and analyzing large datasets from experiments and simulations (88, 89).

Let us first consider the DNN quantification of entanglement in a two-qubit system. The measurement-specific DNNs are fully connected networks. The network has seven fully connected layers with a few dozens of thousands trainable parameters in total. The exact number of the free parameters differs between the networks that have different length of the input vector, dependent on the number of projectors measured. We trained 193 measurement-specific DNNs (12 per point except of full 36 projectors) with varying length of the input layer, starting with the full 36 input neurons down to 4 (with increment of 2).

We construct a set of quantum states as follows: We generate 10^6 random quantum states ρ of which four-fifths are randomly distributed according to the Bures measure induced by the Bures metric (90)

$$\rho = \frac{(1 + U^\dagger)GG^\dagger(1 + U)}{\mathrm{Tr}(1 + U^\dagger)GG^\dagger(1 + U)} \qquad (4)$$

To achieve this, we generate a Ginibre matrix G with complex entries sampled from the standard normal distribution, $G_{ij} \sim \mathcal{N}(0, 1) + i\mathcal{N}(0, 1)$, together with a random unitary U distributed according to the Haar measure (91). The remaining one-fifth of the set consists of random Haar pure states mixed with white

noise. The generation of the set aims at the most uniform and broadest coverage of partially mixed quantum states. The set of quantum states is randomly shuffled and split to two parts, i.e., the training and validation sets containing 800,000 and 200,000 samples, respectively. The test set has 5000 states generated according to the Eq. 4.

For the quantum states, we prepare the corresponding datasets by computing the probability distribution with elements $p_i \equiv \mathrm{Tr}\{\rho M_i\}$ and evaluate the quantum correlation measure (concurrence or mutual information) using Eqs. 1 and 2. We trained the measurement-specific DNNs to predict the quantum correlations from the probability distribution p. The training and validation datasets have the following structures

$$\begin{aligned} \mathscr{D}^{\mathrm{input}} &= \{\mathrm{Tr}\{\rho M_1\}, \ldots, \mathrm{Tr}\{\rho M_{36}\}\} \\ \mathscr{D}^{\mathrm{output}} &= \{\mathscr{Q}(\rho)\} \end{aligned} \qquad (5)$$

where the length of the input vector $\mathscr{D}^{\mathrm{input}}$ is different for various measurement-specific neural networks, ranging from full 36 projectors down to 4. The output $\mathscr{Q}(\rho)$ stands for either the concurrence or the mutual information.

We achieve the learning of the neural networks by backpropagating the error through the use of chain rule of derivation. It minimizes the loss function defined as the mean absolute difference between the true values of the quantum correlations measure $\mathscr{Q}_{\mathrm{true}}$ and the values $\mathscr{Q}^\theta_{\mathrm{predicted}}$ predicted by the networks. The loss function thus takes a form

$$\mathscr{L} = |\mathscr{Q}_{\mathrm{true}} - \mathscr{Q}^\theta_{\mathrm{predicted}}| \qquad (6)$$

and the minimum is found by minimizing the $\mathscr{L}$ over all components of a training dataset to update weights and biases $\{\theta\}$ using the Nesterov-accelerated adaptive moment estimation (NAdam) algorithm. At the step t, the NAdam procedure updates parameters

$$\theta_t \leftarrow \theta_{t-1} - \eta\frac{\overline{\mathbf{m}}_t}{\sqrt{\hat{\mathbf{n}}_t} + \varepsilon} \qquad (7)$$

with

$$\begin{aligned} \mathbf{g}_t &\leftarrow \nabla_{\theta_{t-1}}\mathscr{L}(\theta_{t-1}), \\ \hat{\mathbf{g}} &\leftarrow \frac{\mathbf{g}_t}{1 - \prod_{j=1}^t \mu_j}, \\ \mathbf{m}_t &\leftarrow \mu\mathbf{m}_{t-1} + (1 - \mu)\mathbf{g}_t, \\ \hat{\mathbf{m}}_t &\leftarrow \frac{\mathbf{m}_t}{1 - \prod_{j=1}^{t+1}\mu_j}, \\ \mathbf{n}_t &\leftarrow \nu\mathbf{n}_{t-1} + (1 - \nu)\mathbf{g}_t^2, \\ \hat{\mathbf{n}}_t &\leftarrow \frac{\mathbf{n}_t}{1 - \nu^t}, \\ \overline{\mathbf{m}}_t &\leftarrow (1 - \mu_t)\hat{\mathbf{g}}_t + \mu_{t+1}\hat{\mathbf{m}}_t \end{aligned} \qquad (8)$$

The parameter η represents the learning rate, parameter μ represents the exponential decay rate for the first moment estimates $\hat{\mathbf{m}}$, the parameter ν is the exponential decay rate for the weighted norm $\mathbf{g}_t^2$, and ε is a parameter that ensures the numerical stability of the NAdam optimization procedure. In our work, we set the numerical values of parameters $\{\eta, \mu, \nu, \varepsilon\}$ to $\{0.001, 0.9, 0.999, 10^{-7}\}$. The training takes over 2000 epochs with data further divided into 100 batches to optimize the learning time and accuracy of the

predictions on the validation dataset. All above is implemented using Keras and Tensorflow libraries for Python.

The measurement-independent DNN is a generalization to the measurement-specific DNNs, and, therefore, it consists of single network that predicts the concurrence and the mutual information from any set of projectors that we chose to work with. This functionality is accomplished by a restructuralization of the input layer that inputs not only the vector of probabilities p but also the description of the measurement $\{M_i\}$ itself

$$\mathscr{D}^{\text{input}} = \{M_1, \text{Tr}\{\rho M_1\}, \ldots, M_{36}, \text{Tr}\{\rho M_{36}\}\} \qquad (9)$$

The kernel of the first convolutional layer has a stride length equal to the length of the pair $\{M_i, \text{Tr}\{\rho M_i\}\}$ to prevent the network to see cross-talk between the adjacent input pairs. Each projector M_i is vectorized using d^2 trace orthonormal basis operators $\{\Gamma_i | \Gamma_i \geq 0, \text{Tr}\{\Gamma_i \Gamma_j\} = \delta_{ij} \forall i, j\}$. For incomplete measurements containing less that 36 projectors, we set the values of missing measurement probabilities and projectors to zero.

For the three-, four-, and five-qubit systems, the structure, the loss function, and the optimization procedure of the measurement-specific DNNs are the same as for the systems of two qubits. We trained 44 measurement-specific DNNs for three qubits. The length of the input vector is different for each measurement-specific neural network, ranging from $6^3 = 216$ down to 5. We also trained two specific networks for the four- and five-qubit systems with 325 and 1944 input measurements, respectively. The training and validation datasets are divided in a ratio of 4:1. They contain 100,000 measurement probability distributions (input) and values of the mutual information (output) computed from 100,000 quantum states generated using the same process as for the two-qubit states. The number of training points in the dataset is lower than that in the two-qubit case due to memory limitations. For this reason, we adopted the incremental learning method (92). After the loss function on the validation dataset reaches minimum, which is not updated in the next 200 epochs, the training is stopped, and the best model is saved. Next, we generate different 100,000 data points and continue training. The test set consists of 500 states generated according to Eq. 4.

The complexity of the developed DNNs is rather low, and their scaling to higher-dimensional systems is feasible. The largest network presented (two-qubit device-independent DNN) has almost 460,000 trainable parameters. The five-qubit DNN has slightly more than 230,000 trainable parameters. Its training on 2 million data samples takes 45 hours on a single consumer-grade graphics processing unit. With larger computational resources (available today), we believe that training the networks for entanglement quantification in systems with dozens of qubits should be feasible. The conventional methods, such as MaxLik, are also computationally demanding and have to be evaluated for every new data. In contrast, our approach is computationally demanding only in the training stage. The forward evaluation (from data to entanglement) is computationally easy. Specifically, the DNN entanglement quantification is, on average, four orders of magnitude faster than the MaxLik and two orders of magnitude faster than the SDP.

Experiment

The spontaneous parametric downconversion source consists of a beta barium borate (BBO) crystal cut for type II colinear generation of two correlated orthogonally polarized photons with the central wavelength of 810 nm. The BBO crystal was pumped by a continuous laser. An entangled singlet polarization state was conditionally generated by interfering the correlated photons at a balanced beamsplitter.

To achieve the complete set of data, we performed the full quantum state tomography. This was performed by measuring all 36 projective measurements as combinations of local projections to horizontal, vertical, diagonal, anti-diagonal, right-hand, and left-hand circular polarizations. The polarization analyzer consists of a sequence of half-wave and quarter-wave plates followed by a polarizer, single-mode fiber coupling, and a single-photon detector. The detection events from the two detectors were taken in coincidence basis. To obtain the datasets where the entanglement was reduced by noise, one of the pair photons was propagated through a noisy channel. The noise was implemented by injecting a weak classical signal from an attenuated laser diode. The concurrence of the entangled state reached 0.98 for a short coincidence window and no injected noise. However, for larger coincidence windows and higher levels of injected noise, the concurrence of the detected state decreased. The experimental data for the entangled states with the concurrence of 0.985 ± 0.001 and 0.201 ± 0.002 used in this work were acquired in (93).

Semiconductor quantum dot source consists of a quantum dot embedded in a circular Bragg grating cavity (94) that enables high photon collection efficiency. The quantum dot was excited via two-photon resonant excitation of the biexciton (95). The excitation pulses were derived from a pulsed 80-MHz repetition rate Ti:Sapphire laser. The laser scattering was spectrally filtered, and the exciton and biexciton emission were separated ahead of single-mode fiber coupling. The polarization state of the generated entangled state was analyzed using two polarization analyzers in the process of full quantum state tomography in the same way as it was performed for the parametric downconversion source. The observable degree of entanglement was predominantly limited by the nonzero fine structure splitting.

Supplementary Materials

This PDF file includes:
Supplementary Text
Figs. S1 and S2

REFERENCES AND NOTES

1. R. Horodecki, P. Horodecki, M. Horodecki, K. Horodecki, Quantum entanglement. *Rev. Mod. Phys.* **81**, 865–942 (2009).
2. A. Einstein, B. Podolsky, N. Rosen, Can quantum-mechanical description of physical reality be considered complete? *Phys. Rev.* **47**, 777–780 (1935).
3. J. S. Bell, On the Einstein Podolsky Rosen paradox. *Phys. Phys. Fiz.* **1**, 195–200 (1964).
4. B. Hensen, H. Bernien, A. E. Dréau, A. Reiserer, N. Kalb, M. S. Blok, J. Ruitenberg, R. F. L. Vermeulen, R. N. Schouten, C. Abellán, W. Amaya, V. Pruneri, M. W. Mitchell, M. Markham, D. J. Twitchen, D. Elkouss, S. Wehner, T. H. Taminiau, R. Hanson, Loophole free Bell inequality violation using electron spins separated by 1.3 kilometres. *Nature* **526**, 682–686 (2015).
5. L. K. Shalm, E. Meyer-Scott, B. G. Christensen, P. Bierhorst, M. A. Wayne, M. J. Stevens, T. Gerrits, S. Glancy, D. R. Hamel, M. S. Allman, K. J. Coakley, S. D. Dyer, C. Hodge, A. E. Lita, V. B. Verma, C. Lambrocco, E. Tortorici, A. L. Migdall, Y. Zhang, D. R. Kumor, W. H. Farr,

F. Marsili, M. D. Shaw, J. A. Stern, C. Abellán, W. Amaya, V. Pruneri, T. Jennewein, M. W. Mitchell, P. G. Kwiat, J. C. Bienfang, R. P. Mirin, E. Knill, S. W. Nam, Strong loophole-free test of local realism. *Phys. Rev. Lett.* **115**, 250402 (2015).

6. M. Giustina, M. A. M. Versteegh, S. Wengerowsky, J. Handsteiner, A. Hochrainer, K. Phelan, F. Steinlechner, J. Kofler, J.-Å. Larsson, C. Abellán, W. Amaya, V. Pruneri, M. W. Mitchell, J. Beyer, T. Gerrits, A. E. Lita, L. K. Shalm, S. W. Nam, T. Scheidl, R. Ursin, B. Wittmann, Significant-loophole-free test of Bell's theorem with entangled photons. *Phys. Rev. Lett.* **115**, 250401 (2015).

7. A. Osterloh, L. Amico, G. Falci, R. Fazio, Scaling of entanglement close to a quantum phase transition. *Nature* **416**, 608–610 (2002).

8. T. J. Osborne, M. A. Nielsen, Entanglement in a simple quantum phase transition. *Phys. Rev. A* **66**, 032110 (2002).

9. L. Amico, R. Fazio, A. Osterloh, V. Vedral, Entanglement in many-body systems. *Rev. Mod. Phys.* **80**, 517–576 (2008).

10. H.-S. Zhong, H. Wang, Y.-H. Deng, M.-C. Chen, L.-C. Peng, Y.-H. Luo, J. Qin, D. Wu, X. Ding, Y. Hu, P. Hu, X.-Y. Yang, W.-J. Zhang, H. Li, Y. Li, X. Jiang, L. Gan, G. Yang, L. You, Z. Wang, L. Li, N.-L. Liu, C.-Y. Lu, J.-W. Pan, Quantum computational advantage using photons. *Science* **370**, 1460–1463 (2020).

11. L. S. Madsen, F. Laudenbach, M. Falamarzi. Askarani, T. Vincent, J. F. F. Bulmer, F. M. Miatto, L. Neuhaus, L. G. Helt, M. J. Collins, A. E. Lita, T. Gerrits, S. W. Nam, V. D. Vaidya, M. Menotti, I. Dhand, Z. Vernon, N. Quesada, J. Lavoie, Quantum computational advantage with a programmable photonic processor. *Nature* **606**, 75–81 (2022).

12. S. Wengerowsky, S. K. Joshi, F. Steinlechner, H. Hübel, R. Ursin, An entanglement-based wavelength-multiplexed quantum communication network. *Nature* **564**, 225–228 (2018).

13. J. Yin, Y. H. Li, S. K. Liao, M. Yang, Y. Cao, L. Zhang, J. G. Ren, W. Q. Cai, W. Y. Liu, S. L. Li, R. Shu, Y. M. Huang, L. Deng, L. Li, Q. Zhang, N. L. Liu, Y. A. Chen, C. Y. Lu, X. B. Wang, F. Xu, J. Y. Wang, C. Z. Peng, A. K. Ekert, J. W. Pan, Entanglement-based secure quantum cryptography over 1,120 kilometres. *Nature* **582**, 501–505 (2020).

14. G. Guccione, T. Darras, H. le Jeannic, V. B. Verma, S. W. Nam, A. Cavaillès, J. Laurat, Connecting heterogeneous quantum networks by hybrid entanglement swapping. *Sci. Adv.* **6**, eaba4508 (2020).

15. F. B. Basset, M. Valeri, E. Roccia, V. Muredda, D. Poderini, J. Neuwirth, N. Spagnolo, M. B. Rota, G. Carvacho, F. Sciarrino, R. Trotta, Quantum key distribution with entangled photons generated on demand by a quantum dot. *Sci. Adv.* **7**, eabe6379 (2021).

16. M. Erhard, M. Krenn, A. Zeilinger, Advances in high-dimensional quantum entanglement. *Nat. Rev. Phys.* **2**, 365–381 (2020).

17. J. Eisert, D. Hangleiter, N. Walk, I. Roth, D. Markham, R. Parekh, U. Chabaud, E. Kashefi, Quantum certification and benchmarking. *Nat. Rev. Phys.* **2**, 382–390 (2020).

18. P. Horodecki, Measuring quantum entanglement without prior state reconstruction. *Phys. Rev. Lett.* **910**, 167901 (2003).

19. J. Fiurášek, N. J. Cerf, How to measure squeezing and entanglement of gaussian states without homodyning. *Phys. Rev. Lett.* **93**, 063601 (2004).

20. S. P. Walborn, P. H. S. Ribeiro, L. Davidovich, F. Mintert, A. Buchleitner, Experimental determination of entanglement with a single measurement. *Nature* **440**, 1022–1024 (2006).

21. R. Islam, R. Ma, P. M. Preiss, M. Eric Tai, A. Lukin, M. Rispoli, M. Greiner, Measuring entanglement entropy in a quantum many-body system. *Nature* **528**, 77–83 (2015).

22. A. M. Kaufman, M. E. Tai, A. Lukin, M. Rispoli, R. Schittko, P. M. Preiss, M. Greiner, Quantum thermalization through entanglement in an isolated many-body system. *Science* **353**, 794–800 (2016).

23. R. Filip, Overlap and entanglement-witness measurements. *Phys. Rev. A* **65**, 062320 (2002).

24. A. K. Ekert, C. M. Alves, D. K. L. Oi, M. Horodecki, P. Horodecki, L. C. Kwek, Direct estimations of linear and nonlinear functionals of a quantum state. *Phys. Rev. Lett.* **88**, 217901 (2002).

25. K. Vogel, H. Risken, Determination of quasiprobability distributions in terms of probability distributions for the rotated quadrature phase. *Phys. Rev. A Gen. Phys.* **40**, 2847–2849 (1989).

26. M. Paris, J. Rehacek, Quantum State Estimation (Springer-Verlag, 2004).

27. J. T. Barreiro, N. K. Langford, N. A. Peters, P. G. Kwiat, Generation of hyperentangled photon pairs. *Phys. Rev. Lett.* **95**, 260501 (2005).

28. T. Monz, P. Schindler, J. T. Barreiro, M. Chwalla, D. Nigg, W. A. Coish, M. Harlander, W. Hänsel, M. Hennrich, R. Blatt, 14-Qubit entanglement: Creation and coherence. *Phys. Rev. Lett.* **106**, 130506 (2011).

29. X.-L. Wang, Y. H. Luo, H. L. Huang, M. C. Chen, Z. E. Su, C. Liu, C. Chen, W. Li, Y. Q. Fang, X. Jiang, J. Zhang, L. Li, N. L. Liu, C. Y. Lu, J. W. Pan, 18-Qubit entanglement with six photons' three degrees of freedom. *Phys. Rev. Lett.* **120**, 260502 (2018).

30. D. Gross, Y.-K. Liu, S. T. Flammia, S. Becker, J. Eisert, Quantum state tomography via compressed sensing. *Phys. Rev. Lett.* **105**, 150401 (2010).

31. M. Cramer, M. B. Plenio, S. T. Flammia, R. Somma, D. Gross, S. D. Bartlett, O. Landon-Cardinal, D. Poulin, Y.-K. Liu, Efficient quantum state tomography. *Nat. Commun.* **1**, 149 (2010).

32. G. Tóth, W. Wieczorek, D. Gross, R. Krischek, C. Schwemmer, H. Weinfurter, Permutationally invariant quantum tomography. *Phys. Rev. Lett.* **105**, 250403 (2010).

33. B. P. Lanyon, C. Maier, M. Holzäpfel, T. Baumgratz, C. Hempel, P. Jurcevic, I. Dhand, A. S. Buyskikh, A. J. Daley, M. Cramer, M. B. Plenio, R. Blatt, C. F. Roos, Efficient tomography of a quantum many-body system. *Nat. Phys.* **13**, 1158–1162 (2017).

34. G. Brida, I. P. Degiovanni, A. Florio, M. Genovese, P. Giorda, A. Meda, M. G. A. Paris, A. Shurupov, Experimental estimation of entanglement at the quantum limit. *Phys. Rev. Lett.* **104**, 100501 (2010).

35. G. Brida, I. P. Degiovanni, A. Florio, M. Genovese, P. Giorda, A. Meda, M. G. A. Paris, A. P. Shurupov, Optimal estimation of entanglement in optical qubit systems. *Phys. Rev. A* **83**, 052301 (2011).

36. C. Benedetti, A. P. Shurupov, M. G. A. Paris, G. Brida, M. Genovese, Experimental estimation of quantum discord for a polarization qubit and the use of fidelity to assess quantum correlations. *Phys. Rev. A* **87**, 052136 (2013).

37. D.-L. Deng, X. Li, S. D. Sarma, Quantum entanglement in neural network states. *Phys. Rev. X* **7**, 021021 (2017).

38. G. Carleo, M. Troyer, Solving the quantum many-body problem with artificial neural networks. *Science* **355**, 602–606 (2017).

39. G. Torlai, G. Mazzola, J. Carrasquilla, M. Troyer, R. Melko, G. Carleo, Neural-network quantum state tomography. *Nat. Phys.* **14**, 447–450 (2018).

40. G. Carleo, Y. Nomura, M. Imada, Constructing exact representations of quantum many body systems with deep neural networks. *Nat. Commun.* **9**, 5322 (2018).

41. M. J. Hartmann, G. Carleo, Neural-network approach to dissipative quantum many-body dynamics. *Phys. Rev. Lett.* **122**, 250502 (2019).

42. M. Reh, M. Schmitt, M. Gärttner, Time-dependent variational principle for open quantum systems with artificial neural networks. *Phys. Rev. Lett.* **127**, 230501 (2021).

43. A. Szabó, C. Castelnovo, Neural network wave functions and the sign problem. *Phys. Rev. Res.* **2**, 033075 (2020).

44. T. Westerhout, N. Astrakhantsev, K. S. Tikhonov, M. I. Katsnelson, A. A. Bagrov, Generalization properties of neural network approximations to frustrated magnet ground states. *Nat. Commun.* **11**, 1593 (2020).

45. G. Torlai, R. G. Melko, Latent space purification via neural density operators. *Phys. Rev. Lett.* **120**, 240503 (2018).

46. G. Torlai, B. Timar, E. P. L. van Nieuwenburg, H. Levine, A. Omran, A. Keesling, H. Bernien, M. Greiner, V. Vuletić, M. D. Lukin, R. G. Melko, M. Endres, Integrating neural networks with a quantum simulator for state reconstruction. *Phys. Rev. Lett.* **123**, 230504 (2019).

47. E. S. Tiunov, V. V. Tiunova (Vyborova), A. E. Ulanov, A. I. Lvovsky, A. K. Fedorov, Experimental quantum homodyne tomography via machine learning. *Optica* **7**, 448–454 (2020).

48. A. M. Palmieri, E. Kovlakov, F. Bianchi, D. Yudin, S. Straupe, J. D. Biamonte, S. Kulik, Experimental neural network enhanced quantum tomography. *npj Quantum Inf.* **6**, 20 (2020).

49. O. Danaci, S. Lohani, B. T. Kirby, R. T. Glasser, Machine learning pipeline for quantum state estimation with incomplete measurements. *Mach. Learn. Sci. Technol.* **2**, 035014 (2021).

50. A. Rocchetto, S. Aaronson, S. Severini, G. Carvacho, D. Poderini, I. Agresti, M. Bentivegna, F. Sciarrino, Experimental learning of quantum states. *Sci. Adv.* **5**, eaau1946 (2019).

51. V. Gebhart, R. Santagati, A. A. Gentile, E. M. Gauger, D. Craig, N. Ares, L. Banchi, F. Marquardt, L. Pezzè, C. Bonato, Learning quantum systems. *Nat. Rev. Phys.* **5**, 141–156 (2023).

52. S. Aaronson, in STOC 2018: Proceedings of the 50th Annual ACM SIGACT Symposium on Theory of Computing (Association for Computing Machinery, 2018), pp. 325–338.

53. H.-Y. Huang, R. Kueng, J. Preskill, Predicting many properties of a quantum system from very few measurements. *Nat. Phys.* **16**, 1050–1057 (2020).

54. G. I. Struchalin, Y. A. Zagorovskii, E. V. Kovlakov, S. S. Straupe, S. P. Kulik, Experimental estimation of quantum state properties from classical shadows. *PRX Quantum* **2**, 010307 (2021).

55. S. J. van Enk, C. W. J. Beenakker, Measuring $Tr\rho^n$ on single copies of ρ using random measurements. *Phys. Rev. Lett.* **108**, 110503 (2012).

56. A. Elben, B. Vermersch, M. Dalmonte, J. I. Cirac, P. Zoller, Rényi entropies from random quenches in atomic hubbard and spin models. *Phys. Rev. Lett.* **120**, 050406 (2018).

57. T. Brydges, A. Elben, P. Jurcevic, B. Vermersch, C. Maier, B. P. Lanyon, P. Zoller, R. Blatt, C. F. Roos, Probing Rényi entanglement entropy via randomized measurements. *Science* **364**, 260–263 (2019).

58. A. Elben, S. T. Flammia, H.-Y. Huang, R. Kueng, J. Preskill, B. Vermersch, P. Zoller, The randomized measurement toolbox. *Nat. Rev. Phys.* **5**, 9–24 (2023).

59. P. Horodecki, A. Ekert, Method for direct detection of quantum entanglement. *Phys. Rev. Lett.* **89**, 127902 (2002).

60. J. Fiurášek, Structural physical approximations of unphysical maps and generalized quantum measurements. *Phys. Rev. A* **66**, 052315 (2002).

61. C. Carmeli, T. Heinosaari, A. Karlsson, J. Schultz, A. Toigo, Verifying the quantumness of bipartite correlations. *Phys. Rev. Lett.* **116**, 230403 (2016).

62. O. Gühne, P. Hyllus, D. Bruß, A. Ekert, M. Lewenstein, C. Macchiavello, A. Sanpera, Detection of entanglement with few local measurements. *Phys. Rev. A* **66**, 062305 (2002).

63. M. Barbieri, F. de Martini, G. di Nepi, P. Mataloni, G. M. D'Ariano, C. Macchiavello, Detection of entanglement with polarized photons: Experimental realization of an entanglement witness. *Phys. Rev. Lett.* **91**, 227901 (2003).

64. K. M. R. Audenaert, M. B. Plenio, When are correlations quantum?—Verification and quantification of entanglement by simple measurements. *New J. Phys.* **8**, 266–266 (2006).

65. B. Jungnitsch, T. Moroder, O. Guühne, Taming multiparticle entanglement. *Phys. Rev. Lett.* **106**, 190502 (2011).

66. M. Walter, B. Doran, D. Gross, M. Christandl, Entanglement polytopes: Multiparticle entanglement from single-particle information. *Science* **340**, 1205–1208 (2013).

67. A. Ketterer, N. Wyderka, O. Gühne, Characterizing multipartite entanglement with moments of random correlations. *Phys. Rev. Lett.* **122**, 120505 (2019).

68. L. Knips, J. Dziewior, W. Kłobus, W. Laskowski, T. Paterek, P. J. Shadbolt, H. Weinfurter, J. D. A. Meinecke, Multipartite entanglement analysis from random correlations. *npj Quantum Inf.* **6**, 51 (2020).

69. J. Gao, L. F. Qiao, Z. Q. Jiao, Y. C. Ma, C. Q. Hu, R. J. Ren, A. L. Yang, H. Tang, M. H. Yung, X. M. Jin, Experimental machine learning of quantum states. *Phys. Rev. Lett.* **120**, 240501 (2018).

70. C. Harney, S. Pirandola, A. Ferraro, M. Paternostro, Entanglement classification via neural network quantum states. *New J. Phys.* **22**, 045001 (2020).

71. J. Roik, K. Bartkiewicz, A. Černoch, K. Lemr, Accuracy of entanglement detection via artificial neural networks and human-designed entanglement witnesses. *Phys. Rev. Appl.* **15**, 054006 (2021).

72. D. Kaszlikowski, A. Sen(De), U. Sen, V. Vedral, A. Winter, Quantum correlation without classical correlations. *Phys. Rev. Lett.* **101**, 070502 (2008).

73. M. Miˇuda, R. Stárek, J. Provazník, O. Leskovjanová, L. Mišta, Verifying genuine multipartite entanglement of the whole from its separable parts. *Optica* **6**, 896–901 (2019).

74. D. Lu, T. Xin, N. Yu, Z. Ji, J. Chen, G. Long, J. Baugh, X. Peng, B. Zeng, R. Laflamme, Tomography is necessary for universal entanglement detection with single-copy observables. *Phys. Rev. Lett.* **116**, 230501 (2016).

75. N. Yu, Multipartite entanglement certification, with or without tomography. *IEEE Trans. Inf. Theory* **66**, 6369–6377 (2020).

76. M. A. Valdez, D. Jaschke, D. L. Vargas, L. D. Carr, Quantifying complexity in quantum phase transitions via mutual information complex networks. *Phys. Rev. Lett.* **119**, 225301 (2017).

77. Z. Hradil, J. Řeháˇek, J. Fiurášek, M. Ježek, in Quantum State Estimation (Springer, 2004), pp. 59–112.

78. C. Schwemmer, L. Knips, D. Richart, H. Weinfurter, T. Moroder, M. Kleinmann, O. Gühne, Systematic errors in current quantum state tomography tools. *Phys. Rev. Lett.* **114**, 080403 (2015).

79. G. B. Silva, S. Glancy, H. M. Vasconcelos, Investigating bias in maximum-likelihood quantum-state tomography. *Phys. Rev. A* **95**, 022107 (2017).

80. A. Kalev, R. L. Kosut, I. H. Deutsch, Quantum tomography protocols with positivity are compressed sensing protocols. *npj Quantum Inf.* **1**, 15018f (2015).

81. Z. Hradil, Quantum-state estimation. *Phys. Rev. A* **55**, R1561–R1564 (1997).

82. M. Ježek, J. Fiurášek, Z. Hradil, Quantum inference of states and processes. *Phys. Rev. A* **68**, 012305 (2003).

83. Y. S. Teo, H. Zhu, B.-G. Englert, J. Řeháˇek, Z. Hradil, Quantum-state reconstruction by maximizing likelihood and entropy. *Phys. Rev. Lett.* **107**, 020404 (2011).

84. L. Vandenberghe, S. Boyd, Semidefinite programming. *SIAM Rev.* **38**, 49–95 (1996).

85. Y. LeCun, Y. Bengio, G. Hinton, Deep learning. *Nature* **521**, 436–444 (2015).

86. M. Belkin, D. Hsu, S. Ma, S. Mandal, Reconciling modern machine-learning practice and the classical bias-variance trade-off. *Proc. Natl. Acad. Sci. U.S.A.* **116**, 15849–15854 (2019).

87. K. Kawaguchi, Y. Bengio, L. Kaelbling, in Mathematical Aspects of Deep Learning (Cambridge Univ. Press, 2022), pp. 112–148.

88. G. Carleo, I. Cirac, K. Cranmer, L. Daudet, M. Schuld, N. Tishby, L. Vogt-Maranto, L. Zdeborová, Machine learning and the physical sciences. *Rev. Mod. Phys.* **91**, 045002 (2019).

89. T. Neupert, M. H. Fischer, E. Greplová, K. Choo, M. M. Denner, Introduction to machine learning for the sciences. arxiv:2102.04883 (2021).

90. D. Bures, An extension of Kakutani's theorem on infinite product measures to the tensor product of semifinite $w*$-algebras. *Trans. Am. Math. Soc.* **135**, 199 (1969).

91. F. Mezzadri, How to generate random matrices from the classical compact groups. *Not. Am. Math. Soc.* **54**, 592–604 (2007).

92. G. A. Carpenter, S. Grossberg, D. B. Rosen, Fuzzy ART: Fast stable learning and categorization of analog patterns by an adaptive resonance system. *Neural Netw.* **4**, 759–771 (1991).

93. I. Straka, M. Miková, M. Miˇuda, M. Dušek, M. Ježek, R. Filip, Conditional cooling limit for a quantum channel going through an incoherent environment. *Sci. Rep.* **5**, 16721 (2015).

94. S. Ates, L. Sapienza, M. Davanco, A. Badolato, K. Srinivasan, Bright single-photon emission from a quantum dot in a circular bragg grating microcavity. *IEEE J. Sel. Top. Quantum Electron.* **18**, 1711–1721 (2012).

95. H. Jayakumar, A. Predojević, T. Huber, T. Kauten, G. S. Solomon, G. Weihs, Deterministic photon pairs and coherent optical control of a single quantum dot. *Phys. Rev. Lett.* **110**, 135505 (2013).

Deep learning of quantum entanglement from incomplete measurements

Dominik Koutn, Laia Gins, Magdalena Moczaa-Dusanowska, Sven Hfling, Christian Schneider, Ana Predojevi, and Miroslav Jeek

View the article online
https://www.science.org/doi/10.1126/sciadv.add7131
Permissions
https://www.science.org/help/reprints-and-permissions

Use of this article is subject to the Terms of service